A global digital image correlation enhanced full-field bulge test method

Available online at www.sciencedirect.com

SciVerse ScienceDirect

Procedia IUTAM 4 (2012) 73 – 81

Procedia IUTAM

www.elsevier.com/locate/procedia

Full-field measurements and identification in Solid Mechanics

A Global Digital Image Correlation Enhanced Full-Field Bulge Test Method

J. Neggers[a], J.P.M. Hoefnagels[a,*], F. Hild[b], S. Roux[b], M.G.D. Geers[a]

[a] *Eindhoven University of Technology, Department of Mechanical Engineering, Den Dolech 2, 5612 AZ Eindhoven, The Netherlands*
[b] *LMT Cachan, ENS Cachan / CNRS / UPMC / PRES UniverSud Paris, 61 avenue du Président Wilson, 94235 Cachan Cedex, France*

Abstract

The miniature bulge test is a known method for characterizing the full stress-strain response of freestanding thin films. However, some discrepancies between quantitative results in the literature may be attributed to erroneous assumptions on the bulge shape. In this research, a specialized global Digital Image Correlation technique is developed that circumvents the need for bulge shape assumptions by correlating directly high-resolution profilometry maps of bulged membranes to yield full-field continuous displacement maps, from which local strain maps can be computed. Additionally, local curvature maps are also derived.

Keywords: Bulge test, thin film, displacement measurement, strain and curvature fields

1. Introduction

Thin films are widely utilized in micro-electronic applications, often in multi-layered configurations, comprising different materials with a wide range of mechanical properties [1, 2]. During manufacturing and in-service use the thin film structures may be subjected to large mechanical loads, for instance, due to a mismatch in thermal expansion or in applications such as in flexible displays where flexing or stretching of the device is a product function. It is important to be able to assess the mechanical response of these thin films to predict failure for product reliability optimization. Predictive finite elements simulations, however, require the knowledge of the mechanical behavior of thin films, which may strongly differ from its bulk counterpart because of so-called "size effects." Size effects often occur when one of the geometrical length scales (e.g., the thickness) is of the same order as a micro-structural length scale (e.g., the grain size [3, 4, 5]). Additionally, it has been shown that the mechanical properties of thin films may depend on the substrates they are adhered to [6], typically showing a decrease in strength for free surfaces (e.g., in MEMS applications) and an increase in strength for a (fully) passivated surface (e.g., in multi-layer micro-chips). Consequently, an experimental method is preferred that can test these thin films in the same micro-structural configuration as used in their application. The plane strain bulge test is such a method, being recognized as

*Corresponding author. Phone: +31-40-247-4060; E-mail: j.p.m.hoefnagels@tue.nl

2210-9838 © 2012 Published by Elsevier B.V. Selection and/or peer review under responsibility of H.D. Espinosa and F. Hild.
doi:10.1016/j.piutam.2012.05.022

a powerful experiment that can measure full (isothermal) stress-strain curves, including the plastic regime, of freestanding thin films [7, 8].

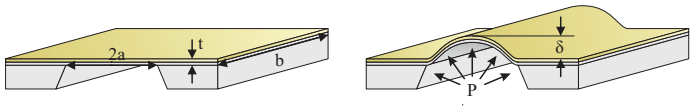

Fig. 1. Schematic views of a plane strain bulge test experiment. A slender rectangular membrane with width $2a$ and thickness t is deflected out-of-plane over a distance δ by a pressure P.

In the plane strain bulge test, a membrane of rectangular shape is deflected by a "lateral" pressure, while the vertical deflection in the center of the membrane is measured, see figure 1. In the conventional analysis, the membrane shape is assumed to be cylindrical, allowing the global stress and strain of the membrane to be approximated by use of the so-called "plane strain bulge equations" [9]

$$\sigma_t = \frac{P}{t\kappa}\,, \tag{1}$$

$$\varepsilon_t = \frac{1}{a\kappa}\sin^{-1}(a\kappa) - 1\,, \tag{2}$$

$$\kappa = \frac{2\delta}{a^2+\delta^2}\,. \tag{3}$$

where σ_t is the tangential membrane stress, ε_t the tangential membrane strain, κ the curvature of the cylindrical part of the membrane, P the applied lateral pressure, t the membrane thickness, a half the membrane width, and δ the deflection of the center of the membrane (figure 1). This theory relies on the assumption of a negligible bending rigidity (i.e., vanishing thickness).

Even though the plane strain bulge test has been widely used and extensively analyzed [10], quantitative results in the literature do not always seem to match. One of the reasons for this discrepancy may be the fact that the real membrane deformation is typically more complex than a purely cylindrical deformation, including (*i*) localized strains close to the boundaries where the membrane is clamped, (*ii*) heterogeneous membrane deformation over the rest of the membrane, i.e., the plane strain state is only found near the center of the rectangular membrane, and (*iii*) the possible effects of anisotropy in the material behavior. None of the above are taken into account in the standard bulge equations.

It would thus be beneficial to develop a method that can measure the full-field stress and strain in a bulged membrane directly from local information away from the boundaries, circumventing the need for a priori assumptions on the membrane deformation and boundary conditions. The present contribution aims at providing such a method. The strategy is based on a full-field topographical measurement of the membrane surface (e.g., confocal surface profilometry, or atomic force microscopy). On the surface a pattern is applied so that Digital Image Correlation (DIC) is used to obtain the full-field displacement. Subsequently, strain and curvature fields are extracted from the surface topography, from which the stress is determined by considering local static equilibrium. To meet this goal, in the current work a custom "global DIC" algorithm is developed that is tailored specifically to be insensitive to micro-fluctuations in the position field for maximum accuracy of the curvature determination, which involves a double derivative of the position field.

2. Experimental Setup

A custom bulge test apparatus is designed and manufactured allowing for the deflection of thin membranes. The apparatus consists of a pressure chamber filled with ethanol. A piston connected to a linear motor acts as the pressure actuator. The apparatus is equipped with three pressure sensors, each with its own working regime, namely, $0 < P < 0.5$ MPa, $0 < P < 1.5$ MPa, and $0 < P < 5$ MPa. The apparatus is small enough to fit underneath the scan-head of, for instance, an optical surface profilometer (figure 2a), in the present case a Sensofar Plμ4200 confocal profilometer.

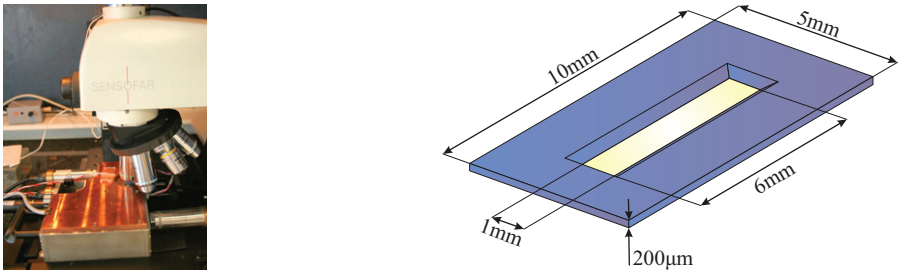

Fig. 2. (a) Photograph of the custom bulge test apparatus when the bulge membrane surface topography is measured with an optical confocal profilometer. (b) Schematic view of the tested samples, a 100 nm thick Si_3N_4 membrane is framed by a 200 µm thick Silicon window.

The experimental technique is validated on bulge experiments of a 100 nm thick Si_3N_4 membrane with a length and width of 1 and 6 mm, respectively (figure 2b). These Si_3N_4 membranes are commercially available products, created with high precision lithographic KOH etching procedures, normally used as Transmission Electron Microscopy (TEM) grids. The well-defined geometry of these membranes and the known material properties of Si_3N_4 make this a well defined test case. Moreover, this bulge membrane is chosen specifically to deform fully elastically and to be largely insensitive to the assumptions made in the bulge equations [11], which allows for an optimum comparison between the conventional bulge test method with its bulge equations and the to-be-developed full-field measurement technique. It should be noted, however, that the bulge equations are often applied to samples far less ideal.

For correlation purposes, a pattern is created by evaporating a solution of 80-500 nm Ag particles in ethanol from the membrane. However, the particles often form clusters of size of a few micrometers. The particles stick to the membrane through physical (Van der Waals) adhesion without influencing the mechanics of the experiment significantly. This is confirmed by the equal response measured using the bulge equation method on a patterned and a non-patterned membrane experiment. Moreover, it is possible to clean the pattern from the membrane using ethanol, indicating no chemical bonding between the particles and the membrane. The measurement sequence consists of incremental loading steps where each time the pressure is increased and then held at a constant pressure. During the constant pressure interval the surface topography of the bulged membrane is acquired using the confocal profilometer, two typical topographies (h_r and h_d) are shown in figure 3.

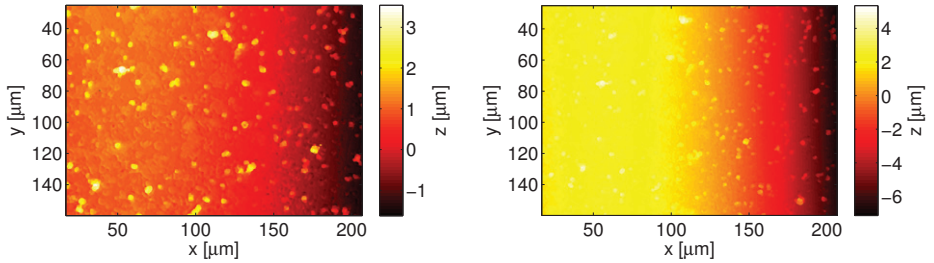

(a) Topography of the reference configuration h_r (b) Topography of the deformed configuration h_d

Fig. 3. Two measured bulge test profiles h_r and h_d, at $P = 0$ MPa and $P = 0.1$ MPa, respectively. A pattern is applied on the surface using micrometer-sized clusters of Ag particles.

3. Global Digital Image Correlation

To obtain the displacement field from the measured surface topographies a custom “global DIC” method is developed. The development is along the same line as prior “global DIC” approaches, described in more

detail in References [12, 13], except for the fact that the current method can deal with the quasi 3D information associated with the surface height topographies of the moving bulge membrane surface, yielding a 3D displacement field as a function of a 2D position vector [14]. The method starts by considering the conservation of topography between a deformed configuration h_d and the corresponding reference configuration h_r

$$h_d\left(\boldsymbol{x} + \boldsymbol{u}_{xy}(\boldsymbol{x})\right) = h_r(\boldsymbol{x}) + u_z(\boldsymbol{x}) + n_o(\boldsymbol{x}) \tag{4}$$

where $\boldsymbol{x}$ is an in-plane coordinate vector, $\boldsymbol{u}_{xy}$ the in-plane displacement, u_z the out-of-plane displacement, and n_o acquisition noise. This conservation is written in its weak form by considering the minimization of the sum of squared height differences over the considered domain

$$\eta^2 = \int \left[h_r(\boldsymbol{x}) - h_d\left(\boldsymbol{x} + \boldsymbol{u}_{xy}(\boldsymbol{x})\right) + u_z(\boldsymbol{x})\right]^2 d\boldsymbol{x} = \int r(\boldsymbol{x})^2 d\boldsymbol{x}, \tag{5}$$

where $r(\boldsymbol{x})$ is the residual field, and η the global residual that is minimized in the global DIC procedure. The displacement field is parameterized as a sum of basis functions $\varphi_n(\boldsymbol{x})$ that act over the entire region of interest and are weighted with a discrete set of degrees of freedom u_n

$$\boldsymbol{u}(\boldsymbol{x}) = u_x(\boldsymbol{x})\boldsymbol{e}_x + u_y(\boldsymbol{x})\boldsymbol{e}_y + u_z(\boldsymbol{x})\boldsymbol{e}_z = \sum_n u_n \varphi_n(\boldsymbol{x})\boldsymbol{e}_i, \tag{6}$$

where $i = \{x, y, z\}$ and the basis functions $\varphi_n(\boldsymbol{x})$ are, for instance, polynomials dependent on the in-plane coordinate $\boldsymbol{x} = x\boldsymbol{e}_x + y\boldsymbol{e}_y$

$$\varphi_n(x, y) = x^{\alpha(n)} y^{\beta(n)}. \tag{7}$$

These basis functions are specifically chosen in this research because the resulting displacement field obtained from the quasi 3D global DIC procedure, which yields the degrees of freedom as output, is continuously differentiable. Such a smooth displacement field is important as the sought stress field is related to the membrane curvature field, which in turn can be obtained by double differentiation of the displacement field, as demonstrated below. Therefore, a continuously differentiable displacement field allows for robust determination of the curvature, or in other words, the measurement noise is effectively filtered out in the quasi 3D global DIC procedure. This is in contrast with a "local" DIC setting, where the displacements of smaller zones of interest are tracked, and the displacement of their centers fitted to a functional form field with a desired (but arbitrary) regularity. A too low level of filtering gives a noisy curvature, whereas a too severe one may depart from the raw result without quantitative indicator on this distance. The main advantage of the global approach is the reduction in the number of unknowns, yet with a form of displacement field that is expected to capture the actual kinematics faithfully. The large support of the chosen basis provides both high robustness and low noise sensitivity.

Note that each basis function (of degree $[\alpha, \beta]$) can be applied in three position directions, associated with three degrees of freedom. For instance, when the basis function of degree $[1, 0]$ (e.g., $\varphi_{10} = x$) is applied in the x-direction it describes a constant normal strain (ε_{xx}), whereas it describes a constant shear strain (ε_{xy}) when applied in y-direction, and a constant tilt in the surface height when applied in the z-direction.

The choice for the number of degrees of freedom should be made carefully. On the one hand, using less degrees of freedom corresponding to a lower polynomial order results in a more robust correlation that is less sensitive to noise. On the other hand, the parameterized displacement field should be rich enough to be able to describe the full kinematics of the membrane deformation in the bulge experiment. Therefore, the minimum number of degrees of freedom should be chosen on consideration of the residual field, $r(\boldsymbol{x})$, which will show systematic deviations from zero when the parameterized displacement field contains insufficient kinematic degrees of freedom. Additionally, it is known that polynomial functions exhibit a loss of conditioning for high polynomial order, α, β, close to the domain boundary. However, for the bulge membrane the highest required polynomial order was 2, and no significant effect was observed. The full list of used basis functions is given in figure 5.

4. Determination of curvature fields

The curvature of a surface, κ_t, in a given direction tangent to the surface, $\boldsymbol{t}$, is equal to the variation of the surface normal vector, $\boldsymbol{n}$, in the tangent direction. Therefore, the curvature is most conveniently calculated from the curvature tensor, $\boldsymbol{\kappa}$, which is the dyadic product of the gradient operator and the normal vector

$$\boldsymbol{\kappa} = \boldsymbol{\nabla} \otimes \boldsymbol{n}, \tag{8}$$

where the gradient operator is given by

$$\boldsymbol{\nabla} = \boldsymbol{e}_x \frac{\partial}{\partial x} + \boldsymbol{e}_y \frac{\partial}{\partial y} + \boldsymbol{e}_z \frac{\partial}{\partial z}. \tag{9}$$

The normal vector is calculated from the position field of the bulge profile, i.e., $z = f(x, y)$, which is obtained from the measured displacement field and is written in the form $F(x, y, z) = f(x, y) - z = 0$, through

$$\boldsymbol{n} = \frac{\boldsymbol{\nabla} F}{\|\boldsymbol{\nabla} F\|}, \tag{10}$$

where $\boldsymbol{\nabla} F$ corresponds to the direction and magnitude of steepest slope. Once the curvature tensor is known, the curvature field in a tangent direction is calculated as

$$\kappa_t(\boldsymbol{x}) = \boldsymbol{t} \cdot \boldsymbol{\kappa} \cdot \boldsymbol{t}, \tag{11}$$

where the unit tangent vector, $\boldsymbol{t}(\boldsymbol{\tau})$, along an in-plane unit vector $\boldsymbol{\tau}(\boldsymbol{x}) = \tau_x \boldsymbol{e}_x + \tau_y \boldsymbol{e}_y$ reads

$$\boldsymbol{t} = \frac{\tau_x \boldsymbol{e}_x + \tau_y \boldsymbol{e}_y + (\boldsymbol{\nabla} f) \cdot \boldsymbol{\tau}\, \boldsymbol{e}_z}{\sqrt{\tau_x^2 + \tau_y^2 + \left[(\boldsymbol{\nabla} f) \cdot \boldsymbol{\tau}\right]^2}}. \tag{12}$$

Often, it is useful to know the maximum and minimum curvatures, which are the principal curvatures, $\kappa_1(\boldsymbol{x})$ and $\kappa_2(\boldsymbol{x})$, in the direction of the (unit) principal curvature vectors, $\boldsymbol{t}_1(\boldsymbol{x})$ and $\boldsymbol{t}_2(\boldsymbol{x})$. This means that the principal curvatures and principal curvature directions are the eigenvalues and eigenvectors of the curvature tensor and are thus obtained through a diagonalization of the curvature tensor. Vectors $\boldsymbol{t}_1(\boldsymbol{x})$ and $\boldsymbol{t}_2(\boldsymbol{x})$ are perpendicular to each other and tangent to the surface, i.e., $\boldsymbol{t_1} \times \boldsymbol{t_2} = \boldsymbol{n}$. It is to be observed that in general, the computation of the curvature involves geometrical non-linearities, as shown above, which have to be taken into account if the slope of the bulge becomes significant.

5. Synthetic Bulge Test

The new methods are first applied to a synthetic experiment, to allow for the verification of the procedure without having to deal with measurement uncertainties. Only one half of the membrane is modeled with a Finite Element model using 15,000 8-node quadratic thick shell elements. The material model used is elastic in a large displacement formulation, where the material parameters of Si_3N_4 are chosen (i.e., Young's modulus of $E = 235$ GPa, and Poisson's ratio of $\nu = 0.27$). The mesh was tested for mesh convergence and, in fact, the current number of elements used is larger then necessary, to yield a finer spacing for the differentiation steps that are needed to obtain the curvature fields.

From the simulation, but also in the experiment, the initial (nodal) positions and the incremental displacements are recorded, which yields the surface height profile as a function of the initial in-plane position vector. Therefore, an additional numerical interpolation step is applied to obtain the surface height profile as a function of the current position vector, which is required when using equation (10). Subsequently, the normal vector field and curvature tensor are obtained by numerical differentiation using equation (10) and (8), respectively. The tangent vector fields in x- and y-direction are obtained with equation (12), and the curvature fields in x- and y- direction with equation (11). These fields are plotted in figure 4 together with the topography. Note that, in the plane strain area, the curvatures in the x- and y-directions match what

is expected from the bulge equations, i.e., $\kappa_x \approx 0.42$ mm^{-1} and $\kappa_y \approx 0$ mm^{-1}, and match the curvatures obtained from the integration points of the shell elements (figure 4e-h).

It is to be emphasized that the present numerical simulation was performed in a more general framework than the membrane approximation used to derive the "bulge equations" (1-3). The presented result not only validates the applicability of the membrane approximation for the problem at hand, but also shows that the edge effect due to the finite extension of the rectangular geometry only affects a narrow region whose extent is of the order of the bulge film width. The above results demonstrate that the curvature fields can be obtained correctly also in a numerical environment and with the additional numerical interpolation step, which gives confidence for the determination of the curvature fields from the experimental quasi 3D global DIC data as discussed next.

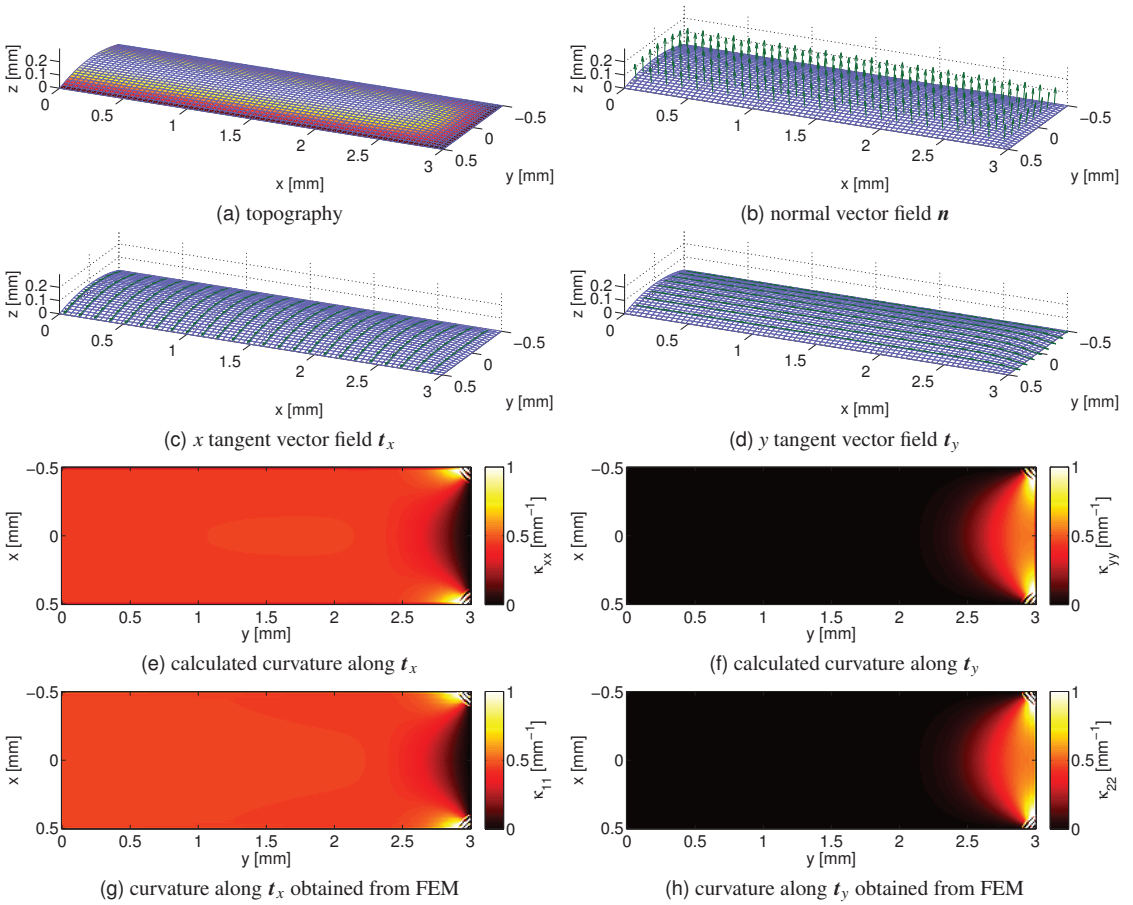

Fig. 4. Synthetic experiment where one half of the bulge membrane is simulated using a finite element model.

6. Experimental results

The newly-developed quasi 3D global DIC procedure with a parameterized displacement field with 12 degrees of freedom is applied to the series of surface height profiles (in the plane-strain region of the bulge) as a function of bulge pressure, as shown in figure 3, in order to obtain the change of the 3D displacement field. As an example, figure 5 shows the three components of the 3D displacement field, as obtained for the bulge membrane at a pressure of $P = 0.1$ MPa. As above mentioned, the quality of the correlation can be checked from the residual field, $r(\boldsymbol{x})$, which is also shown in figure 5. The residual field shows some local peaks around the Ag particles, which are naturally present due to the fact that the membrane rotates with increasing pressure resulting in a change of effective viewing angle of the particles with the

surface height profilometry. Apart from these local peaks, no systematic deviation from zero is found in the residual field, thereby indicating that the parameterized displacement field with 12 degrees of freedom contains sufficient kinematic freedom to describe the membrane deformation, namely, the measurement of the quasi 3D displacement field is successful.

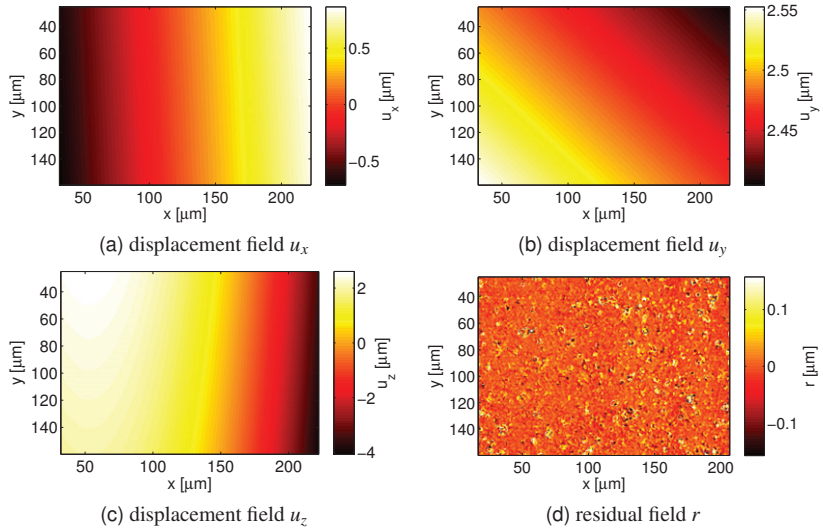

Fig. 5. (a,b,c) Displacement fields in x-, y-, and z-directions obtained from the DIC procedure. (d) Residual field r, which shows the correlation error when using 12 shape functions, namely $[\alpha,\beta] = \{[0,0],[1,0],[0,1],[2,0]\}$ for the x-direction, $[\alpha,\beta] = \{[0,0],[1,0],[0,1]\}$ for the y-direction and $[\alpha,\beta] = \{[0,0],[1,0],[0,1],[2,0],[0,2]\}$ for the z-direction.

The method to obtain the curvature fields is applied to the measured position and displacement fields, for which the results are shown in figure 6. Even though the curvatures (and deflections) are very small, the normal and tangent vector fields are obtained correctly. More importantly, since the measurement result only contains data from the plane strain part of the membrane, the obtained curvature fields are nearly constant and match the results from the bulge equations and the synthetic experiment. Only the curvature along the x- and y-axes are shown as the cross term, κ_{xy} is essentially 0 over most of the analyzed domain. Let us stress that the proposed analysis shows that the curvature along the membrane longitudinal axis is vanishingly small. This is important, since the bulge equations assume that this curvature is null (i.e., plane strain assumption). The proposed procedure thus indicates if this assumption is satisfied on the observed field of view. In such a case, the balance equation allows stress measurements to be performed without an assumption on the constitutive law. Interestingly, no measurement noise seems to be visible, i.e., all the obtained results are perfectly smooth. This is because, in the global DIC procedure, only smooth displacement fields are considered.

A quantitative analysis of the effect of noise has been performed but is not documented herein. The latter analysis allows to design the most appropriate order of polynomials to be used for the best compromise in terms of flexibility of the analysis to capture the actual displacement field, and noise sensitivity with respect to the chosen quantity of interest and its location.

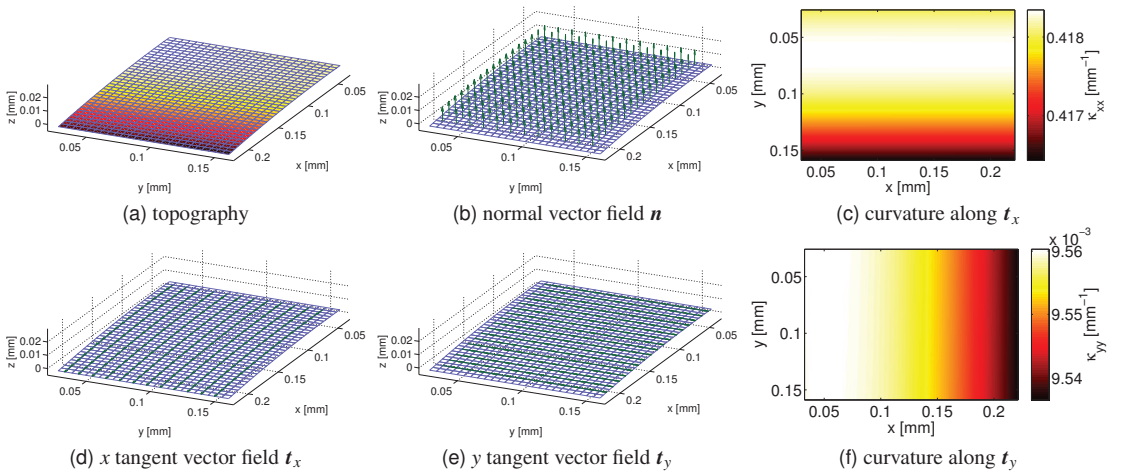

(a) topography (b) normal vector field $\boldsymbol{n}$ (c) curvature along $\boldsymbol{t}_x$

(d) x tangent vector field $\boldsymbol{t}_x$ (e) y tangent vector field $\boldsymbol{t}_y$ (f) curvature along $\boldsymbol{t}_y$

Fig. 6. Experimental results taken at a pressure increment of $P = 0.1$ MPa

7. Conclusions

A custom version of global Digital Image Correlation has been developed to cope with the 3D nature of the surface profilometry data, where the gray-level has the meaning of z-position. First, a bulge tester has been miniaturized to fit underneath a microscope, e.g., a confocal optical profilometer, enabling for full-field surface topography measurements of a bulging membrane. The newly-developed 3D global DIC method yields full-field displacement maps of the bulging membrane and utilizes a long wavelength discretization basis to enforce a smooth and continuously differentiable measured displacement field. This makes it possible to calculate the membrane curvature field from the double derivative of the position field with high accuracy.

Both the displacement measurement and the curvature calculation have been tested on a simulated finite element method synthetic experiment, and a proof of principle experiment performed under conditions known to be well approximated by the bulge equations, to which the experimental measurements have been compared. The results from these studies give confidence that the method can be used to capture the three-dimensional displacement fields and curvature fields of bulge membranes without using any a priori knowledge on the kinematics, relieving the need for the bulge equations with its associated assumptions. The method will be further developed to be able to capture full-field stress and strain maps, the details of which are still under development.

References

[1] W.D. Nix, *Mechanical properties of thin films*, Metallurgical transactions A, vol 20A, 2217-2245 (1989)
[2] R.P. Vinci and J.J. Vlassak, *Mechanical behavior of thin films*, Annual Review of Materials Science, Vol. 26, 432-462 (1996)
[3] J.R. Greer, W.C. Oliver and W.D. Nix, *Size dependence of mechanical properties of gold at the micron scale in the absence of strain gradients*, Acta Materialia, Vol. 53, 1821-1830 (2005)
[4] P.A. Gruber, J. Böhm, F. Onuseit, A. Wanner, R. Spolenak, E. Arzt, *Size effects on yield strength and strain hardening for ultra-thin Cu films with and without passivation: A study by synchrotron and bulge test techniques*, Acta Materialia, Vol. 56, 2318-2335 (2008)
[5] E. Arzt, *Size effects in materials due to microstructural and dimensional constraints: a comparative review*, Acta Materialia, Vol. 46-16, 5611-5626 (1998)
[6] L.B. Freund and S. Suresh, *Thin film materials: stress, defect formation, and surface evolution*, Cambridge University Press, New York, (2003)
[7] J.J. Vlassak and W.D. Nix, *A new bulge test technique for the determination of Young's modulus and Poisson's ratio of thin films*, Journal of Materials Research, Vol. 7-12, 3242-3249 (1992)
[8] Y. Xiang, J.J. Vlassak, *Bauschinger and size effects in thin-film plasticity*, Acta Materialia, Vol. 54, 5449-5460 (2006)
[9] Y. Xiang, X. Chen, J.J. Vlassak, *Plane-strain bulge test for thin films*, Journal of Materials Research, Vol. 20-9, 2360-2370 (2005)

[10] M.K. Small and W.D. Nix, *Analysis of the accuracy of the bulge test in determining the mechanical properties of thin-films*, Journal of Materials Research, Vol. 7, 1553-1563 (1992)
[11] J. Neggers, J.P.M. Hoefnagels and M.G.D. Geers, *On the Validity Regime of the Bulge Equations*, Journal of Materials Research, DOI: 10.1557/jmr.2012.69 (2012)
[12] G. Besnard, F. Hild and S. Roux, *Finite-element displacement fields analysis from digital images: Application to Portevin-Le Châtelier bands*, Experimental Mechanics, 46, 141-157 (2006)
[13] F. Hild, S. Roux, N. Guerrero, M. E. Marante, J. Flórez-López, *Calibration of constitutive models of steel beams subject to local buckling by using digital image correlation*, European Journal of Mechanics A/Solids 30, 1e10 (2011)
[14] K. Han, M. Ciccotti, S. Roux, *Measuring Nanoscale Stress Intensity Factors with an Atomic Force Microscope*, EuroPhysics Letters, Vol. 89, 66003 (2010)